Low-threshold electron emission from diamond

J. B. Cui, J. Ristein, and L. Ley
Institute of Technical Physics, University of Erlangen-Nürnberg, Erwin-Rommel-Strasse 1, D-91058 Erlangen, Germany
(Received 22 March 1999)

We have studied the photoassisted electron emission of single-crystal diamond (111) for photon energies from just above the diamond band gap of 5.5 eV well into the sub-band-gap regime ($h\nu \approx 2.8$ eV). As an independent parameter, the electron affinity was varied between -1.27 eV [negative electron affinity (NEA)] and $+0.38$ eV [positive electron affinity (PEA)] by changing the hydrogen coverage of the surface. A substantial sub-band-gap emission band with constant intensity is observed in all cases. Except for the NEA surfaces, it dominates the electron flux. We attribute this intense band to nanometer-size graphitic patches which cover less than 1% of the surface area. The low-energy threshold for this emission band is, however, not determined by intrinsic properties of graphite, but controlled by the work function of the surrounding diamond matrix. The details of this inhomogeneous emission model, which may have implications for the field emission from nanocrystalline diamond films, are discussed. [S0163-1829(99)08647-6]

I. INTRODUCTION

In diamond research, the characterization and understanding of electron emission is playing an increasingly important role because of its implication for diamond as a cold cathode emitter and as a photocathode. These particular applications are possibly related to the unique property of diamond, namely its negative electron affinity (NEA). NEA enables electrons at the conduction-band minimum to escape from the diamond without an energy barrier at the surface. This has been shown to enhance the photoelectron yield considerably and may also have beneficial consequences for the field emission of diamond-based devices.

As far as such field emission applications of diamond films are concerned, considerable technological progress has been achieved recently with emission thresholds as low as 0.5 V/μm for polycrystalline diamond.[1] Despite these achievements, the microscopic field emission process is far from being understood.[2] In general, it appears that ''bad'' diamond material has superior field emission properties in terms of threshold voltage and current density. Bad in this context implies microcrystalline or nanocrystalline diamond phases embedded in or mixed with nondiamond phases such as amorphous or graphitic carbon.

Photoelectron yield spectroscopy (Yield) is one of the important methods to study the electron emission process in diamond. Yield is defined as the number of electrons emitted from a surface per incident photon. The relevance of yield spectroscopy to the characterization of diamond as a photocathode material is obvious. As far as the field emission properties are concerned, Yield contributes to the elucidation of one step in the whole field emission process, namely the transport of electrons to and their escape from the surface of diamond. Important contributions to these aspects using yield spectroscopy come from the work of Bandis and Pate, who concentrated on emission originating from the excitation of excitons and free electrons by light energies at and above the band gap of diamond.[3] However, high sensitivity yield spectroscopy by Ristein *et al.*[4] and Cui *et al.*[5] has revealed non-negligible contributions of electron emission also at subband-gap light energies that have been attributed to electrons excited from defects in CVD diamond films as well as IIb single crystals.

In this paper we present a systematic study of the yield spectra of single-crystal diamond (111) with the electron affinity or work function as an independently controlled parameter. The electron affinity was taken from $\chi = -1.3$ to $+0.38$ eV by controlled desorption of hydrogen from an initially fully hydrogenated surface. Through a quantitative analysis of the spectra that covers the below- and above-band-gap regime simultaneously, we come to the conclusion that the dominant part of the sub-band-gap emission originates in graphitic patches at the surface. The emission threshold from these patches is lowered substantially compared to that of bulk graphite on account of the NEA of the surrounding diamond. For reasons to be discussed in Sec. IV, we consider this result relevant for the field emission process in nanocrystalline diamond films.

II. EXPERIMENTAL DETAILS

The sample used in this study is a type-IIb single-crystal diamond with a (111) surface of 3×5 mm^2. The diamond sample is boron doped with a concentration of about 10^{16} cm^{-3} and has a conductivity of about 1 Ω^{-1} cm^{-1}, which is sufficiently high to avoid surface charging in our experiments.

The sample treatment is identical to that adopted in our earlier photoemission work.[4,5] It consists in a hydrogenation of the crystal in a microwave plasma which produces well-ordered hydrogen-terminated surfaces exhibiting a sharp (1×1) low-energy electron-diffraction (LEED) pattern with a low background. They are free of any contaminants other than H and possibly C as judged by x-ray excited photoelectron spectroscopy (XPS).

The diamond sample was clamped to a Ta foil and heated by electron-beam bombardment from the back of the Ta sample holder. The true temperature of the diamond was measured with an accuracy of ± 10 K by Raman spectroscopy as explained in Ref. 6.

TABLE I. Annealing sequence of the diamond (111) surface.

Annealing step no.	Temperature (K)	Duration (min)	accumulated annealing time at 1000 K (min)
1	625	8	
2	750	10	
3	820	10	
4	1000	12	12
5	1000	12	24
6	1000	18	42
7	1000	12	54
8	1000	12	66
9	1000	12	78
10	1000	25	103
11	1000	20	123

The yield spectra were measured in UHV for photon energies between 2.0 and 6.2 eV. A high-sensitivity, high signal-to-noise ratio, and large dynamic range up to eight orders of magnitude in the Yield were achieved by a reduction of stray light to better than 10^{-9} and optimized electron optics with a collection efficiency for the photoelectrons which is close to unity. Details of the experimental setup are given in Ref. 7. The spectra reported here were all measured under identical conditions and are thus comparable on a relative scale.

In addition, XPS and work-function measurements by the Kelvin method were routinely performed after each annealing step in order to determine the position of the Fermi level at the surface, the work function, and the electron affinity as described in Ref. 5.

III. RESULTS

The hydrogenated diamond sample was taken through a series of annealing steps ending with an isothermal annealing sequence at 1000 K (see Table I). After each step the sample was left to cool in UHV down to RT before the XPS and yield spectra were recorded and the work function measured.

In the course of the first two annealing steps at temperatures below 800 K (see Table I), the subband-gap part of the yield spectrum undergoes a substantial change as shown in Fig. 1. An emission band with a threshold of about 2 eV which is present on the as-hydrogenated surface is removed. Such a band has earlier been observed on CVD diamond films[4] and its origin is presently under investigation. After the third annealing at 820 K, the shape of the subband-gap part of the spectrum remains unchanged except for a rigid shift towards higher photon energies with annealing time.

Up to an annealing time of 42 min at 1000 K, the yield exhibits a steep rise at the band-gap energy of diamond (5.5 eV) that is characteristic for a surface with negative electron affinity (NEA).[3–5] NEA is the result of the hydrogen coverage of the surface. After an annealing time of 66 min, the hydrogen coverage has dropped below its critical value of about 10% of a monolayer.[8] The surface turns from NEA to positive electron affinity (PEA) and the sharp rise in the yield at 5.5 eV disappears.

The Yield of the NEA surface in the region of the band-gap energy as shown in Fig. 2 confirms the close relationship

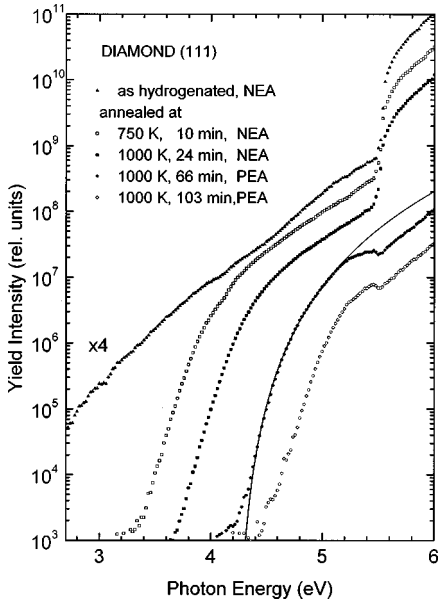

FIG. 1. Photoelectron yield spectra taken on the as-hydrogenated diamond (111) surface and after several annealing steps (see Table I). The annealing temperature and time and the electron affinity (NEA or PEA) are indicated in the figure. The solid line is an empirical fit of the sub-band-gap emission corresponding to Eq. (1).

of this part of the yield spectrum with the optical absorption of diamond that has been noticed and analyzed earlier by Bandis and Pate[3] and by Ristein *et al.*[4] Upon closer scrutiny we observe, however, subtle changes in the spectral shape as we proceed with the annealing and—more important—substantial changes in the magnitude of the yield (note the logarithmic scale in Fig. 2) despite the fact that the surface remains NEA. An explanation of these observations will be offered in Sec. IV.

Returning to the subband-gap region we first ascertain that the spectral shape and the intensity of this emission band remain unchanged after the first two annealing steps for photon energies below 5.25 eV. This is demonstrated in Fig. 3, where the last four spectra of Fig. 1 are superimposed on top of each other after they have been rigidly shifted in photon energy. The shifts are set by visual inspection but turn out to be equal to the change in work function as will be discussed immediately. The photon energy of 5.25 eV is indicated for each spectrum by a vertical line. The spectral shape in the subband-gap regime is well described by a power law.

$$Y(E) = A(E - E_{\mathrm{th}})^4 \tag{1}$$

as demonstrated by the solid line in Fig. 1. Here E and E_{th} refer to the photon energy and the threshold energy, respectively, and A is the ''amplitude'' of the emission intensity.

Kane[10] has analyzed the photoelectron yield threshold of semiconductors and semiconductor surfaces under all conceivable circumstances regarding the shape and dimensionality of the bands involved and the presence or absence of k-vector conservation in the emission process. He did indeed find power-law thresholds with exponents between 1 and $\frac{5}{2}$ but never 4. We therefore consider Eq. (1) a mere parametrization of the spectral shape in order to extract the threshold energy E_{th} and the amplitude parameter A. Also shown in

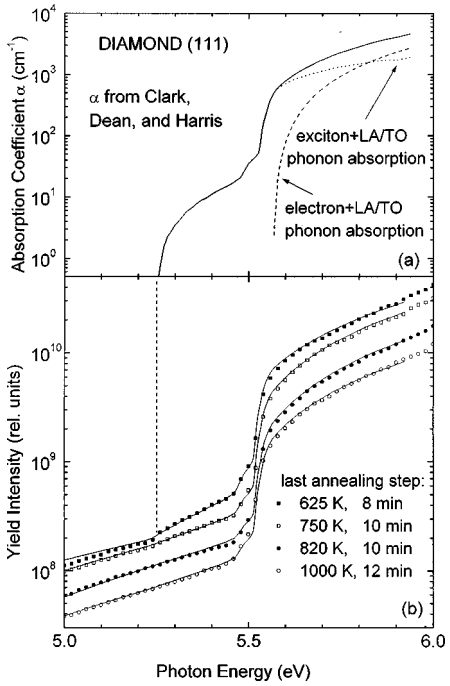

FIG. 2. Absorption coefficient (a) and the fine structure of photoelectron yield spectra (b) of the diamond (111) surface after the first few annealing steps. The absorption coefficient α is from Clark, Dean, and Harris (Ref. 9) and was confirmed by our own measurements below $h\nu = 5.6$ eV. The dashed and dotted line in (a) are the main contributions of electrons and excitons, respectively, which are due to the simultaneous excitation of the quasiparticles together with an LA or TO phonon (not resolved). Roughly two orders of magnitude weaker is the absorption band with the lowest threshold energy (vertical dashed line), which is connected with exciton excitation and LA/TO phonon deexcitation. In (b), the squares and circles are the experimental data points and the solid lines are the fits by the sum of Eqs. (2) and (5).

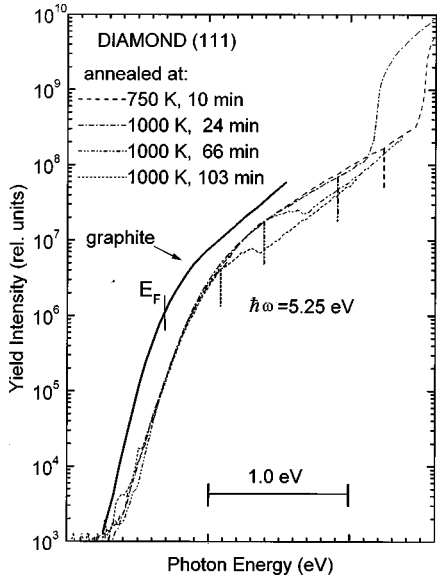

FIG. 3. Photoelectron emission spectral shape for NEA and PEA diamond (111) surfaces. The spectra were shifted with respect to each other along the energy axis without scaling their intensities. The solid line represents the emission spectrum of graphite. The vertical bars indicate the photon energy of 5.25 eV for each diamond spectrum. For the graphite spectrum we have indicated the photon energy which just corresponds to the onset of transitions from the Fermi level (E_F).

Fig. 3 is the yield spectrum of HOPG graphite as measured by Schäfer *et al.*,[11] which resembles the subband-gap emission of diamond closely and we shall return to this resemblance later.

The diamond spectra in Fig. 3 have been superimposed without scaling their intensities and it is apparent that their amplitudes are remarkably constant in the sub-band-gap regime. Fits of this part of the spectra to Eq. (1) yield parameters A that are plotted as a function of the thermal history of the sample in Fig. 4(a). The amplitude A turns out to be entirely independent of the state of the surface including the transition from NEA to PEA.

Most significantly, the *changes* in the threshold energies $E_{\rm th}$ that were also obtained from the fits are identical to the changes in work function as demonstrated in Fig. 4(b). The change in work function, $\Delta\phi = \Delta\chi - \Delta(E_F - E_V)$, as a function of annealing time is mainly brought about via variation of the electron affinity by a thermally activated desorption of hydrogen and the concomitant loss in surface dipole density as elaborated elsewhere.[5]

IV. DISCUSSION

A. Analysis of the yield spectra in the band-gap regime

We will start the discussion of our results by concentrating first on the yield spectra in the band-gap range ($h\nu > 5.25$ eV) and deal with the sub-band-gap emission later. The photoelectron yield at and above the band gap of diamond has previously been modeled in terms of a three-step process involving the bulk optical excitation of electron-hole pairs proportional to the absorption coefficient α, transport of the electrons to the surface, and emission through the surface into vacuum with a certain probability P. The transport to the surface is controlled by a characteristic length l which describes the probability $e^{-x/l}$ that a carrier created at a depth x below the surface will reach the surface. It is furthermore necessary to distinguish between the creation, transport, and escape of excitons (subscript ''ex'') and electrons (subscript ''e'') so that the Yield due to intrinsic absorption can be written

$$Y_B = \frac{P_e l_e \alpha_e(h\nu)}{1 + l_e \alpha(h\nu)} + \frac{P_{\rm ex} l_{\rm ex} \alpha_{\rm ex}(h\nu)}{1 + l_{\rm ex}\alpha(h\nu)}. \qquad (2)$$

This formula is the result of an integration over the depth-dependent generation rate $g_{e,\rm ex}(x) = I_0(1-R_1)e^{-\alpha x}\alpha_{e,\rm ex}$ and the corresponding transport expression of the carriers to the surface, all for an incoming photon flux I_0 that is reduced by the surface reflectivity R_1. The constant α in Eq. (2) which determines the exponential attenuation of the light flux in the diamond is just the sum of the partial absorption constants, i.e., $\alpha(h\nu) = \alpha_e(h\nu) + \alpha_{\rm ex}(h\nu)$. For the excitons, it is of course further required that they break up at the surface in order to release the electron as a photoelectron; this additional restriction can be considered as included in the escape probability $P_{\rm ex}$.

Yield spectra of diamond NEA surfaces have been successfully described in the band-gap regime using Eq. (2) with parameters l and P, which are independent of energy.[3]

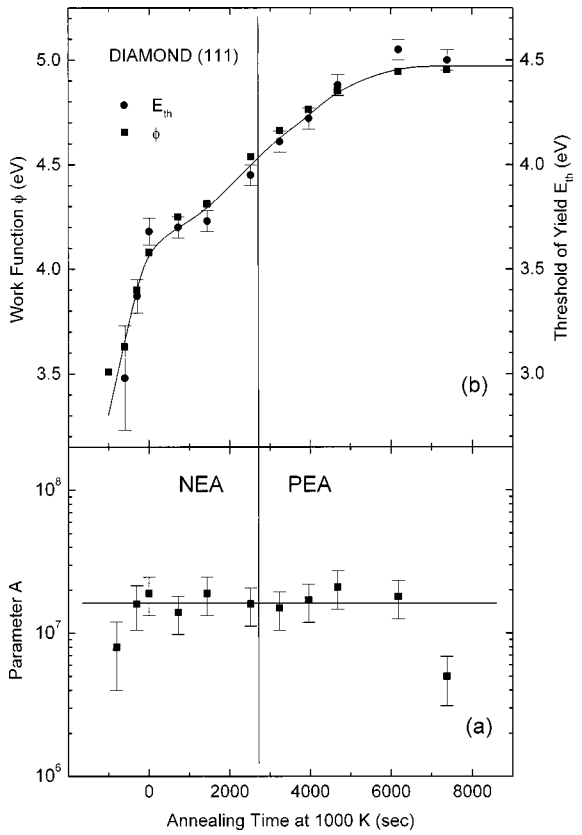

FIG. 4. Emission amplitude parameter A (a) and work function ϕ and yield threshold E_{th} (b) as a function of annealing time. The yield threshold and parameter A were obtained by fitting the experimental spectra to Eq. (1) below 5.25 eV. The vertical line indicates the point where the electron affinity is zero.

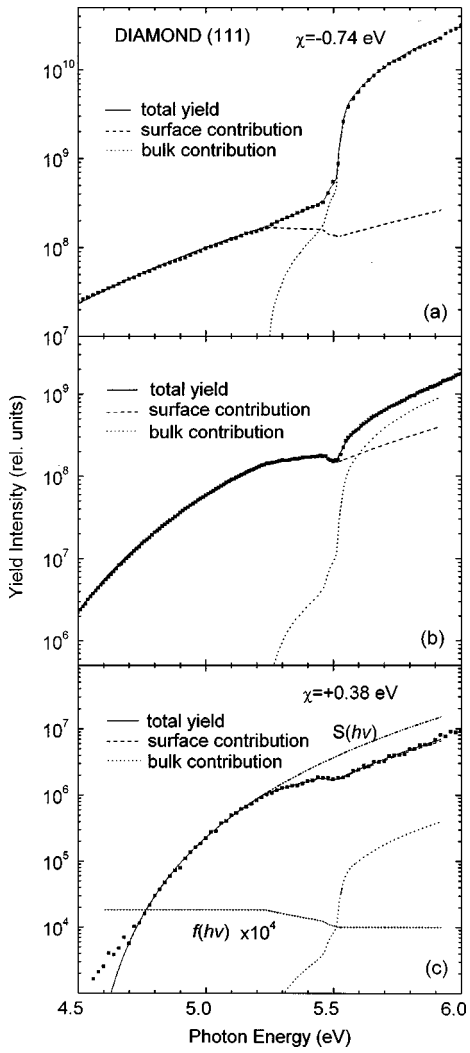

FIG. 5. Fits to the yield spectra of diamond surfaces with NEA (a) and (b) and PEA (c) by combining Eqs. (2) and (5). The solid squares are the experimental data points and the solid lines are the fitting results. The dashed and dotted lines represent the surface and bulk contributions, respectively. In (c) the spectral function $S(h\nu)$, and $f(h\nu)$ from Eq. (3) are also plotted.

For NEA surfaces, $l_{e,\mathrm{ex}}$ corresponds to $L_{e,\mathrm{ex}}$, the diffusion length of electrons (excitons), because the majority of carriers thermalize to the conduction-band minimum and reach the surface by diffusion.

With a minor modification in the meaning of the partial absorption constant $\alpha_{e,\mathrm{ex}}(h\nu)$, in that optical excitation processes into final conduction-band states below the vacuum level have to be excluded, Eq. (2) remains valid in the case of PEA. In this case, $l_{e,\mathrm{ex}}$ is the inelastic mean free path $\lambda_{e,\mathrm{ex}}$ because electrons have to reach the surface essentially without energy loss in order to overcome the surface barrier $\chi > 0$. The mean free path $\lambda_{e,\mathrm{ex}}$ is orders of magnitude smaller than $L_{e,\mathrm{ex}}$ and this is the reason why the above-band-gap yield is so much higher on NEA than on PEA surfaces (compare Fig. 1). Since the electron mean free path λ ($\sim$ a few hundred Å) is substantially smaller than the penetration depth α^{-1} of light ($\alpha^{-1} > 2\ \mu$m, see Fig. 2), $\alpha(h\nu)\lambda \ll 1$, and the intrinsic yield spectrum of diamond reduces to the weighted sum of the partial absorption constants in the case of PEA.

The fits of the photoyield spectra from the NEA surfaces displayed in Figs. 2 and 5 were achieved on the basis of Eq. (2) augmented by a sub-band-gap contribution that will be discussed in the next section. In the fits, the products $P_{e,\mathrm{ex}} l_{e,\mathrm{ex}}$ were kept as free parameters and the agreement with the experimental data confirms that Eq. (2) models the band-gap contribution of the photoelectron emission from NEA diamond surfaces correctly.

B. Analysis of the sub-band-gap regime

For a complete understanding of our results, we have to include the sub-band-gap contribution to the photoyield spectra as well. In a previous publication[4] we had assumed that the excitation of electrons from bulk defects into the conduction band in conjunction with the large diffusion length in type-IIb single-crystal diamond ($L_{e,\mathrm{ex}} = 200\ \mu$m) is responsible for the subband-gap contribution of NEA surfaces. In this case the photoemission threshold coincides with the energy separation between the defect level and the conduction-band minimum (CBM). Our new results, which prove unambiguously that the threshold of the subband-gap emission tracks the work function for both NEA and PEA surfaces as the hydrogen coverage varies, make this interpretation virtually untenable. In particular, the CBM of diamond can no longer be involved in the emission process of this part of the

yield spectrum. We are thus left with two possibilities. Either the photoemission process proceeds via direct optical excitation from diamond surface states (intrinsic or defect related) to outgoing vacuum states (homogeneous direct emission model), or we are dealing with photoemission from a separate phase other than diamond at the surface (inhomogeneous emission model). In the latter case we have to explain the connection of the photoemission threshold of this phase with the vacuum level over the diamond part of the sample. As will be discussed below, experimental evidence strongly favors the second explanation.

For both models the emission intensity is proportional to the light intensity at the surface $I_s = I_0(1-R_1)f(h\nu)$. The function of $f(h\nu)$ takes the contribution of multiply reflected light in the sample into account. In the incoherent limit it reads

$$f(h\nu) = \frac{1+R_2 e^{-2\alpha(h\nu)d}}{1-R_1R_2e^{-2\alpha(h\nu)d}}. \tag{3}$$

Here R_1 is the reflection coefficient for the diamond surface and R_2 is the effective reflectivity of the back surface including the Ta sample holder. For the narrow spectral range of interest we can ignore the photon energy dependence of R_1 and R_2 and the values of $R_1 = 0.22$ from Ref. 12 and of $R_2 = 0.6$.[12(a)] $\alpha(h\nu)$ and d are the absorption coefficient and the thickness of the sample, respectively. The function f varies from 1.8 to 1.0 significantly only in the range where $\alpha(h\nu)$ is comparable to the thickness of the sample [$5.25 \leqslant h\nu \leqslant 5.53$ eV, see Fig. 5(c)]. This variation reflects the decrease of the light intensity at the surface as soon as reflections from the back side of the sample are attenuated by the onset of the fundamental absorption of diamond. Naturally, multiple reflections have to be taken into account for the band-gap contribution Y_B as well. However, calculations show that here the effect is at most 10% and it has therefore been neglected in Eq. (2).[4,13] The subband-gap mechanism thus contributes as

$$Y_s(h\nu) = S(h\nu)f(h\nu) \tag{4}$$

to the total yield spectrum. The spectral function $S(h\nu)$ has a different meaning for the two models. For the inhomogeneous emission model $S(h\nu) = P_s\lambda_s\alpha_s(h\nu)$, where $\alpha_s(h\nu)$ is the partial absorption constant for the optical excitation, λ_s the mean free path of the electrons, and P_s a quantum efficiency for the surface emission, all parameters appropriate for the foreign nondiamond phase.

For the homogeneous direct emission model $S(h\nu) = P_sN_s\sigma_s(h\nu)$, where $\sigma_s(h\nu)$ is the absorption cross section, N_s the lateral density of the surface states, and P_s again a quantum efficiency for electron emission.

For $h\nu < 5.25$ eV, $f(h\nu)$ is constant and equals 1.8. In this photon energy range the shape of the spectral function is thus given directly by the Yield and it was shown to be represented by $S(h\nu) = A'(E-E_{\rm th})$.[4] Using the same spectral function over the whole photon energy range, we have

$$Y_S = f(h\nu)A'(E-E_{\rm th})^4 \tag{5}$$

with $A' = A/1.8$. By adding bulk and surface contributions according to Eqs. (2) and (5) we could fit the whole set of experimental photoyield spectra over the complete spectral range. Examples of the fits in the critical region near E_g are shown by the solid lines in Fig. 2 for a series of NEA surfaces and in Fig. 5 for the transition from NEA to PEA. The excellent quality of all fits over the whole range of electron affinities is apparent and even subtle spectral features such as the gradual loss of the phonon assisted threshold at 5.25 eV in Fig. 2 and the development of the minimum in Fig. 5 are faithfully reproduced with only $P_e l_e$ and $P_{\rm ex} l_{\rm ex}$ as free parameters for the bulk contribution.

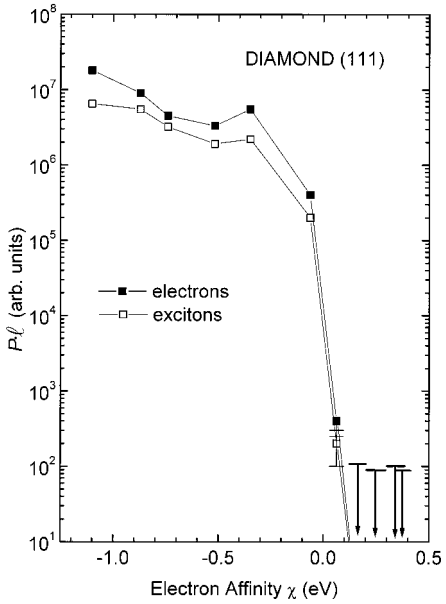

FIG. 6. Change in *Pl* as a function electron affinity. The values of *Pl* were obtained from fits. For PEA ($\chi > 0$) no significant band-gap contribution can be identified by the fits and therefore only an upper limit for *Pl* can be obtained.

These two parameters as extracted from our fits are plotted as a function of the electron affinity of the surface in Fig. 6. Without knowing the absolute value of the photoyield, we can only specify relative values of *Pl* for both quasiparticles. For the surfaces with NEA this quantity is on average a factor of 2.5 larger for excitons than for electrons and both decrease by a factor of about 50 between the lowest (-1.1 eV) and the highest (-0.06 eV) negative electron affinity.

As explained in Ref. 4, the escape probability P is given by

$$P = \frac{S_{\rm em}}{S_{\rm em}+S_{\rm rec}+\mu_D}, \tag{6}$$

where $S_{\rm em}$, $S_{\rm rec}$, and μ_D are, respectively, the surface recombination, the surface emission, and the diffusion velocity. As has been shown for silicon, the surface recombination velocity is dramatically reduced when surface dangling bonds are passivated by hydrogen.[14] In analogy it is not unlikely that $S_{\rm rec}$ on diamond increases with increasing electron affinity because the latter is connected with the loss of hydrogen coverage as explained in Ref. 8. Thus as the hydrogen desorbs from the surface, χ increases and at the same time P decreases because of the increasing surface recombination velocity.

After the transition from NEA to PEA, the products *Pl* are at least five orders of magnitude smaller than for the surface

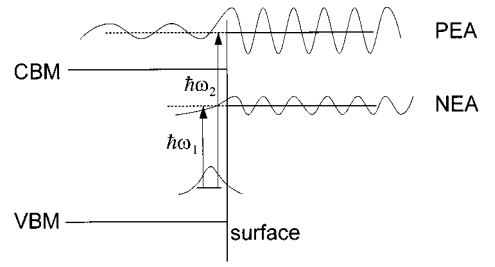

homogeneous emission model

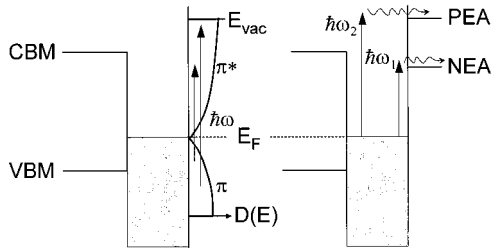

inhomogeneous emission model

FIG. 7. Schematic diagrams of the wave functions, densities of states $D(E)$, and energies involved in the homogeneous (upper panel) and the inhomogeneous (lower panel) electron emission model, respectively.

with NEA reflecting the switchover from $l_i = L_i$ (diffusion length) to $l_i = \lambda_i$ (inelastic-scattering length).

C. Model for the subband-gap emission

We now turn to the discussion of the two possible models for the subband-gap emission process, which have already been outlined briefly above. The most important argument in favor of the inhomogeneous emission model is displayed in Fig. 4. On the one hand, the threshold of the subband-gap emission tracks the work function over the whole range of electron affinities; on the other hand, the emission intensity of the band is independent of the electron affinity. The homogeneous emission model relies on an optical transition between a localized surface state and a final state at the vacuum level. The corresponding final-state wave functions undergo a dramatic change when the electron affinity changes sign (see Fig. 7). They are semi-infinite in the case of NEA, i.e., extended *in vacuo* but exponentially decaying into the diamond because there are no matching energy levels in the fundamental gap. However, when the surface turns to PEA the final states at threshold and above have finite amplitudes *in vacuo and* within the crystal since they are degenerate with bulk conduction-band states. It is inconceivable that the transition probability from a surface state is unaffected by such a dramatic change in the final-state wave function. In fact, no significant difference in yield is observed when the diamond surface changes from NEA to PEA, which disagrees with the expectation of the direct emission model.

This contradiction does not occur in the inhomogeneous emission model, where the sub-band-gap emission originates in patches of a different material at the diamond surface. The patches are large enough (at least several hundred atoms) to develop their own band structure and the classical three-step process for photoemission applies as indicated in the lower panel of Fig. 7. In addition, the experimental results shown in Fig. 4(b) also suggest that the states which are responsible for the low-threshold emission have a fixed energy with respect to the surface Fermi level. A natural candidate for this second phase is amorphous or graphitic carbon. Extended graphitic patches have earlier been invoked to explain chemically shifted C 1*s* core-level spectra[15] and the pinning of E_F after annealing of diamond above 1300 K.[8]

The identification of the nondiamond phase responsible for the sub-band-gap photoyield spectrum as being graphite (or sp^2-rich amorphous carbon, which has similar electronic properties) is supported by the comparison of the diamond yield spectra with that of graphite (HOPG) in Fig. 3.

The electronic structure of a graphitic patch on diamond is sketched schematically in the lower panel of Fig. 7 (left-hand side). Indicated is the semimetallic density of states $D(E)$ of graphite with occupied π and empty π^* states that touch at the Fermi level E_F. If we accept for the time being that the vacuum level for the graphitic patches varies as indicated on the lower right-hand panel of Fig. 7, the photoemission process from these patches is in all cases essentially that of a semimetal with a work function varying between 3.5 (NEA) and 5.0 eV (PEA). For this reason we do not expect drastic changes in the shape or amplitude of the graphitic part of the yield spectrum as a function of the position of the vacuum level. This is in fact what we observe for the sub-band-gap part of the yield spectra and it explains the unusual spectral shape (for a semiconductor) which nevertheless resembles that of HOPG graphite. For HOPG with a work function of 5.0 eV the fitting procedure [Eq. (1)] as applied to all sub-band-gap yield spectra yields an apparent threshold $E_{\mathrm{th}} = 4.6$ eV. The difference between ϕ and E_{th} is due to the thermal occupation of states above E_F and is well known from the photoyield of metals.[16] Thus in the conventional language the observed lowering in the photoemission threshold from the graphitic patches (see Fig. 4) implies a corresponding reduction in the work function by about 1.5 eV as compared to intrinsic graphite. The only remaining challenge is to explain why the vacuum level which is relevant for the emission from the graphitic patches is determined by the electron affinity of the surrounding diamond surface.

D. The photoemission threshold energy

In order to illustrate the concept of work-function reduction on an inhomogeneous surface, we have sketched schematically the surface potential in the vicinity of a lateral diamond-graphite heterojunction for the case of the lowest EA of $\chi = -1.27$ eV ($\phi = 3.5$ eV) in Fig. 8. For simplicity we assume a circular graphitic patch as shown by the top view in Fig. 8(a). The geometry of this triple junction (diamond, graphite, and vacuum) renders the commonly presented one-dimensional band diagrams inappropriate for the region where the three interfaces meet (point *C*). At the top of the cross-section view in Fig. 8(b), we have plotted the conventional band diagram for the diamond surface which holds well away from the diamond-graphite boundary. The

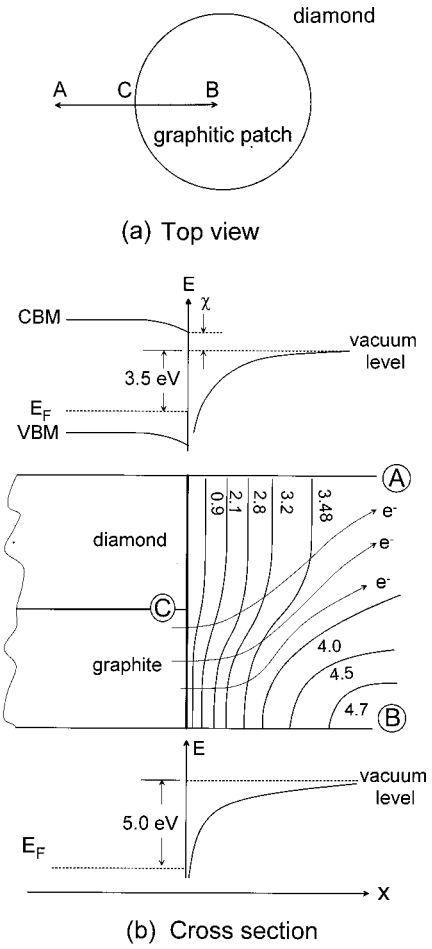

FIG. 8. Schematic diagram of the potential distribution in front of a sample in the framework of the inhomogeneous electron emission model. (a) Top view, (b) cross section. In the top and bottom parts of (b) the band diagrams for diamond and graphite are given. In the middle of (b) the potential in front of the sample and near the diamond/graphitic patch border *C* is given in the form of equipotential lines.

surface Fermi-level position of 0.68 eV above the VBM is known from the C 1*s* binding energy[8] and the bulk Fermi-level position of 0.37 eV above the VBM is calculated from the acceptor concentration of our diamond sample. This yields the downward surface band bending, as is commonly observed. On the vacuum side we have indicated qualitatively the image potential experienced by an electron that leaves the diamond surface. Asymptotically this potential approaches a value that differs by the work function of diamond from the Fermi energy. The image potential varies over a distance of about 20 Å and the asymptotic value is commonly referred to as the vacuum level.[17] Note that in conventional band diagrams the explicit form of the image potential is not drawn and just its asymptotic value is given in the form of the vacuum level. Since diamond is the dominant surface phase, the electron affinity relevant in the band diagram on the upper part of the cross section is identical to the one we have measured as an average over the whole sample. Note that the width of the depletion layer, i.e., the range of band bending inside the diamond, is of the order of 2500 Å. Thus the scale of the position axis inside and outside the sample has to be interpreted as different by two orders of magnitude.

At the bottom of Fig. 8(b) we have constructed the same diagram for the surface of the graphitic patch, again sufficiently far away from the diamond-graphite boundary. Since graphite is a semimetal, the valence- and conduction-band edges coincide at the Fermi level and band-bending effects are irrelevant on the length scale of the diagram. The work function of graphite of 5.0 eV was used to place E_{vac} in this diagram.

The center part of Fig. 8(b) represents a plane that is perpendicular to the diamond surface and the interface between diamond and the graphitic patch. In this plane we have drawn the image potential in the form of equipotential lines with the Fermi level as a common zero extending from the center of the graphitic patch [in Fig. 8(a)] outwards. Away from the interface the equipotential lines run parallel to the surface and represent the image potential as shown in the band diagrams at the top and bottom of Fig. 8(b), respectively. Over the boundary between diamond and the graphitic patch, the equipotential lines have to join smoothly as indicated. The difference in work function between diamond and the graphitic material gives rise to a contact potential difference of 1.5 eV. Therefore, an electron starting from point *A* over the diamond surface and going to point *B* over the graphitic patch has to overcome the contact potential difference by crossing the equipotential lines that bend away from the surface as indicated in the figure.

From the construction of equipotential lines in Fig. 8(b), it is evident that electrons emitted form the graphitic patches near the boundary with the diamond are able to escape into vacuum without having to overcome the 5-eV work function of graphite. In fact, electrons that leave the graphitic patch within a certain range of the boundary see effectively the work function of diamond. This range is approximately equal to the variation length of the image potential perpendicular to the surface (~20 Å). Some of the trajectories that electrons are expected to follow are indicated in Fig. 8. The equipotential lines above 3.5 eV (the work function of the diamond) will eventually loop around symmetrically with respect to the center line in Fig. 8(b) and thus form a potential barrier in front of the graphitic patch. The lateral extent of the barrier and its height is reduced as the size of the graphitic patch shrinks. For patch diameters considerably less than about 40 Å, the barrier disappears and all electrons emitted from the graphitic patches have an emission threshold that varies with the work function of diamond, as it is observed experimentally.

Summarizing the preceding discussion, the inhomogeneous emission model offers a mechanism by which the material that provides the electrons for emission into the vacuum is different from that which determines the energy barrier at the surface.

Finally we would like to stress that the graphitic patches on our single-crystal diamond sample account for less than 1% of the surface area as estimated from the graphite contribution to the C 1*s* core-level spectrum measured by XPS.[15]

V. CONCLUSION

The systematic study of low-energy electron emission from diamond presented here has important implications for

the field emission mechanism of diamond-based material. Two specific features of our experiment are different from all other experiments related to the issue of field emission. First, we have used a single-crystal diamond surface on which the electron affinity and the work function could be measured reliably and controlled systematically by gradual dehydrogenation. Second, we have adopted subband-gap photoexcitation as a tool to determine the threshold energy for electron emission spectroscopically, i.e., without relying on the interpretation of current voltage characteristics.

Our results show that the dominant electron emission near threshold from a diamond surface is due to graphitic patches on the surface, which provide a finite density of electrons at the Fermi level. Diamond is neither involved in the optical excitation nor (which is more important for field emission) in the transport of the electrons to the surface. However, being by far the dominant surface phase, diamond determines the energy barrier for all electrons which attempt to leave the surface from the graphitic phase. In this inhomogeneous electron emission process, the role of diamond is reduced to an agent that controls the effective work function, which is as low as 3.5 eV for a fully hydrogen covered surface. This value results from a low electron affinity of $\chi = -1.27$ eV and a downward surface band bending of 0.3 eV. Although the graphitic patches that provide the electrons for vacuum emission cover less than 1% of the total surface area of our diamond sample, they are nevertheless the sole source of sub-band-gap photoelectron emission.

The situation encountered for single-crystal diamond will hold *a fortiori* in polycrystalline or nanocrystalline CVD diamond films where sp^2-bonded carbon decorates the grain boundaries. It is observed that nanocrystalline diamond films make excellent field emitters after they have been treated in a hydrogen atmosphere.[18] Furthermore, it is found that the threshold field decreases with grain size[19] and Wang *et al.*[20] observed emission to occur at the boundaries between diamond grains and the sp^2-bonded nondiamond phase in between. We therefore suggest that, notwithstanding other consideration, the inhomogeneous emission model should be considered in any field emission theory of diamond-based systems. In this model, the diamond phase provides a (thermally and mechanically) stable matrix with a comparatively low work function and the graphitic phase provides the transport path for electrons to the surface.

ACKNOWLEDGMENTS

The authors thank M. Stammler for the plasma preparation of the diamond surfaces. This work was supported by the Deutsche Forschungsgemeinschaft under Contract No. DFG Le 634/5-3 and carried out under the auspices of the trinational ''D-A-CH'' cooperation of Germany, Austria, and Switzerland on ''Synthesis of Superhard Materials.''

[1] K. Okano, S. Koizumi, S. R. P. Silva, and G. A. J. Amaratunga, Nature (London) **381**, 140 (1996).
[2] See, for example, R. Schlesser, M. T. McClure, B. L. McCarson, and Z. Sitar, Diamond Relat. Mater. **7**, 639 (1998).
[3] C. Bandis and B. Pate, Phys. Rev. B **52**, 12 056 (1995); Phys. Rev. Lett. **74**, 777 (1995).
[4] J. Ristein, W. Stein, and L. Ley, Phys. Rev. Lett. **78**, 1803 (1997); W. Stein, J. Ristein, and L. Ley, Diamond Relat. Mater. **7**, 626 (1998).
[5] J. B. Cui, J. Ristein, and L. Ley, Phys. Rev. Lett. **81**, 429 (1998).
[6] J. B. Cui, K. Amtmann, J. Ristein, and L. Ley, J. Appl. Phys. **83**, 7929 (1998).
[7] J. Schäfer, J. Ristein, L. Ley, and H. Ibach, Rev. Sci. Instrum. **64**, 653 (1993).
[8] J. B. Cui, J. Ristein, and L. Ley, Phys. Rev. B **59**, 5847 (1999).
[9] C. D. Clark, P. J. Dean, and P. V. Harris, Proc. R. Soc. London, Ser. A **277**, 312 (1964).
[10] Evan O. Kane, Phys. Rev. **127**, 131 (1962).
[11] J. Schäfer, J. Ristein, and L. Ley, J. Non-Cryst. Solids **164–166**, 1123 (1993).
[12] *Numerical Data Functional Relationships in Science and Technology*, Landolt-Börnstein New Series, Vol. 17, edited by K.-H. Hellwege (Springer-Verlag, Berlin, 1982), p. 375. (a) The value of $R2$ is calculated by considering the multireflection between diamond and Ta sample holder. The reflection coefficient of Ta is from J. H. Weaver, D. W. Lynch, and C. G. Olson, Phys. Rev. B **10**, 501 (1973).
[13] J. Ristein (unpublished).
[14] E. Yablonovitch, D. L. Allara, C. C. Chang, T. Gmitter, and T. B. Bright, Phys. Rev. Lett. **57**, 249 (1986).
[15] R. Graupner, F. Maier, J. Ristein, L. Ley, and Ch. Jung, Phys. Rev. B **57**, 12 397 (1998).
[16] R. H. Fowler, Phys. Rev. **38**, 45 (1931).
[17] Th. Fauster and W. Steinmann, in *Photonic Probes of Surfaces*, edited by P. Halevi (Elsevier, Amsterdam, 1995), p. 347.
[18] W. Zhu, G. P. Kochanski, and S. Jin, Science **282**, 1471 (1998).
[19] W. Zhu, G. P. Kochanski, S. Jin, and L. Seibles, J. Appl. Phys. **78**, 2707 (1995).
[20] C. Wang, A. Garcia, D. Ingram, M. Lake, and M. E. Kordesch, Electron Device Lett. **27**, 1459 (1991).